


# Fluorinated 2D Lead Iodide Perovskite Ferroelectrics

Tai-Ting Sha, Yu-An Xiong, Qiang Pan, Xiao-Gang Chen, Xian-Jiang Song, Jie Yao, Shu-Rong Miao, Zheng-Yin Jing, Zi-Jie Feng, Yu-Meng You,\* and Ren-Gen Xiong

Hybrid perovskite materials are famous for their great application potential in photovoltaics and optoelectronics. Among them, lead-iodide-based perovskites receive great attention because of their good optical absorption ability and excellent electrical transport properties. Although many believe the ferroelectric photovoltaic effect (FEPV) plays a crucial role for the high conversion efficiency, the ferroelectricity in  $\text{CH}_3\text{NH}_3\text{PbI}_3$  is still under debate, and obtaining ferroelectric lead iodide perovskites is still challenging. In order to avoid the randomness and blindness in the conventional method of searching for perovskite ferroelectrics, a design strategy of fluorine modification is developed. As a demonstration, a nonpolar lead iodide perovskite is modified and a new 2D fluorinated layered hybrid perovskite material of  $(4,4\text{-difluorocyclohexylammonium})_2\text{PbI}_4$ , **1**, is obtained, which possesses clear ferroelectricity with controllable spontaneous polarization. The direct bandgap of 2.38 eV with strong photoluminescence also guarantees the direct observation of polarization-induced FEPV. More importantly, the 2D structure and fluorination are also expected to achieve both good stability and charge transport properties. **1** is not only a 2D fluorinated lead iodide perovskite with confirmed ferroelectricity, but also a great platform for studying the effect of ferroelectricity and FEPV in the context of lead halide perovskite solar cells and other optoelectronic applications.

Recently, hybrid organic–inorganic perovskites (HOIP) have been attracting increasing attention due to their great application potential in photovoltaics, optoelectronics, and piezoelectrics.<sup>[1]</sup> Especially in photovoltaics, the power conversion efficiency (PCE) of perovskite solar cells (PSC) is boosting from 3.8%<sup>[2]</sup> to 24.2%<sup>[3]</sup> in just few years. The high PCE and advantages of low-cost, easy fabrication, flexibility, etc. grant them the title of “wonder materials” and make them a potential candidate in next generation of photovoltaic materials.<sup>[4,5]</sup> In high performance PSC, the light absorbing material is normally lead-based hybrid perovskites, such as the most famous methylammonium lead iodide ( $\text{MAPbI}_3$ ), due to their good optical property,

T.-T. Sha, Y.-A. Xiong, Q. Pan, X.-G. Chen, X.-J. Song, J. Yao, S.-R. Miao, Z.-Y. Jing, Z.-J. Feng, Prof. Y.-M. You, Prof. R.-G. Xiong  
Jiangsu Key Laboratory for Science and Applications of Molecular Ferroelectrics  
Southeast University  
Nanjing 211189, P. R. China  
E-mail: youyumeng@seu.edu.cn

 The ORCID identification number(s) for the author(s) of this article can be found under <https://doi.org/10.1002/adma.201901843>.

DOI: 10.1002/adma.201901843

electrical transport performance, and long carrier lifetime. Besides these factors, the ferroelectric photovoltaic effect (FEPV) was also believed to contribute to the good performance in PSC.<sup>[6]</sup> Conventional photovoltaic devices utilize heterojunctions to create asymmetric electric potential to separate the photoinduced charge carriers. While, for FEPV, the photogenerated electron–hole pair is separated by the spontaneous polarization or domain walls in homogeneous ferroelectric materials.<sup>[7]</sup> Since FEPV is independent to the bending of energy band, it can generate extremely large open-circuit voltage comparable to the bandgap and is expected to enhanced efficiency in PSC. Although FEPV draws a very exciting picture, the ferroelectricity of  $\text{MAPbI}_3$  is still controversial.<sup>[8]</sup> To study the detailed contribution of FEPV in PSC, obtaining a lead-iodide-based polar perovskite materials with settled ferroelectricity is very necessary as a useful complement to the current PSC materials and model system to investigate the role of ferroelectric polarization in photovoltaics.

Besides the intensive competition on PCE, PSC are facing a more severe problem of stability. During operation, the applied electric field or optoelectrical field may induce migration of organic molecules and halogen ions. Even without light and electric field, in ambient condition, the moisture and oxygen may also decompose the perovskite.<sup>[9]</sup> Those factors limit the lifetime of PSC for only  $\approx 1000$  h, which is far away from that of conventional silicon-based solar cell panel (20–25 years). One possible solution to this problem is reducing the dimensionality from 3D to quasi-2D, which has large formation energy, high moisture stability, and long lifetime, however, such low-dimensional perovskite will affect transport properties and reduce PCE.<sup>[5,10]</sup> Until very recently, fluorination on 2D lead iodide perovskite was reported to enhance charge transport and PCE.<sup>[11]</sup> Thus, in order to achieve a good balance between PCE and stability, a fluorinated 2D lead iodide perovskite ferroelectric material is highly demanded, which is also a good platform to study the fundamental mechanism behind high PCE.

Although we have reported several lead-based perovskite ferroelectrics with 2D layered structure, the ferroelectricity can only coexist with chlorine or bromine, even slight doping of iodine would alter the crystal structure and vanish the precious ferroelectric property.<sup>[12]</sup> Until now, rational design and synthesis of HOIP ferroelectrics is still very challenging and

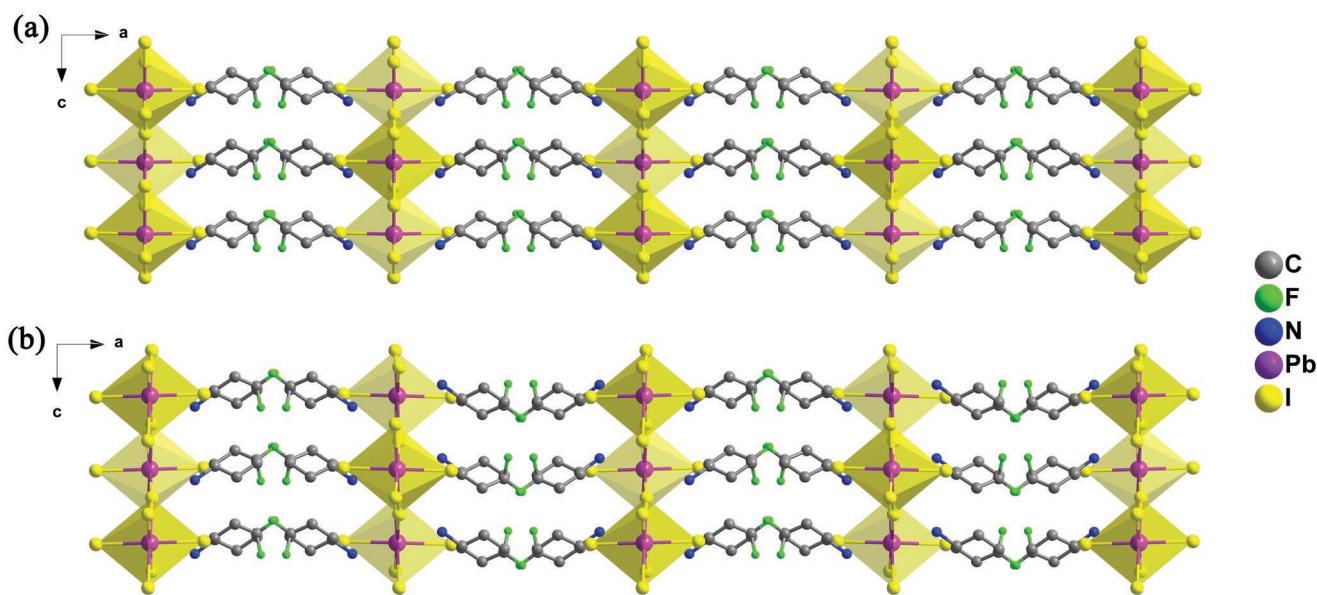


**Figure 1.** a,b) The packing view of **1** at 298 K (a) and 398 K (b), projected along the *b*-axis. Hydrogen atoms are omitted for clarity.

most approaches rely on random screening. In order to avoid the randomness and blindness, we developed a rational design strategy of fluorine modification to obtain ferroelectric lead iodide perovskites. By properly substituting the hydrogen by the fluorine on the organic component of a hybrid lead iodide perovskite, we can convert the original centrosymmetric compound to the noncentrosymmetric polar material and attribute ferroelectricity to the 2D lead iodide perovskite. In this report, we utilized the fluorine modification method, and obtained the first fluorinated 2D lead iodide perovskite of (DFCHA)<sub>2</sub>PbI<sub>4</sub> (DFCHA = 4,4-difluorocyclohexylammonium), **1**, with robust ferroelectricity and a direct bandgap as low as 2.38 eV. The lead iodide and the DFCHA cation stacked alternatively to form a layered 2D perovskite structure. At temperature below Curie point (*T<sub>c</sub>*) of 377 K, **1** exhibits good ferroelectric hysteresis characteristic, and more importantly, the polarization switching has been successfully demonstrated by “double wave” method and directly visualized by microscopic imaging. The lead iodide does provide not only frameworks to stabilize the crystal structure, but also a direct bandgap with optical absorption edge of 514 nm, which attribute good optical absorption and emission properties to **1**. Furthermore, our careful investigation confirmed the relationship between photogenerated current and ferroelectric polarization, which directly prove the existence of FEPV and exhibit the great potential of **1** in PSC and other optoelectronic applications.<sup>[13]</sup>

By simple solution synthesis, single crystals of **1** can be obtained in good quality, with a general formula of A<sub>2</sub>BX<sub>4</sub>, where monovalent organic ammonium A is intercalated between anion of inorganic lead halide sheets of BX<sub>4</sub>. Such a layered 2D structure not only provides structural complexity to fine tune the optical properties, but also allows adjustment of ferroelectricity and functionalities separately. Since ferroelectricity can only be found for materials crystallized in 10 polar point groups, crystallographic structures are critical to determine the possibility of ferroelectricity and corresponding

polarization properties. In order to probe the crystallographic structure, we carried out single-crystal X-ray diffraction study on the obtained crystalline sample of **1**. Similar to previously reported 2D hybrid perovskites, at temperature higher than the Curie point, **1** is in the centrosymmetric high temperature phase (HTP), and the crystal structure can be refined as the nonpolar space group of *Pbca* (the detailed crystallographic information can be found in Table S1, Supporting Information). As shown in **Figure 1**, each 2D sheet consists of infinite corner-sharing PbI<sub>6</sub> octahedra, and the orderly packed DFCHA cations occupy the space between sheets, as that of a typical Ruddlesden–Popper perovskite structure. Each layer of lead iodide is sandwiched by two layers of organic cations with N closing to the nearest lead iodide sheet due to the Coulomb interaction. To be noticed, in HTP, the two layers of DFCHA adjacent to every lead iodide sheet are centrosymmetric to each other. Thus the anisotropy of DFCHA is cancelled out and the HTP is a nonpolar paraelectric phase. When **1** is at room temperature, it is in the low temperature phase (LTP), which crystallizes in the polar space group of *Cmc2<sub>1</sub>* with crystal cell parameters similar to those of HTP. Comparing to the structure in HTP, half of DFCHA cations reorient during the phase transition and break the inversion symmetry, thus a macroscopic polarization can be expected in such an arrangement. Such a phase transition is one of the 88 species of ferroelectric phase transition as concluded by Aizu with notation of *mmmFmm2*.<sup>[14]</sup>

We examined the typical and significant changes of related properties of **1** around *T<sub>c</sub>* by differential scanning calorimetry (DSC) (Figure S1a, Supporting Information), temperature-dependent second harmonic generation (SHG) (Figure S1b, Supporting Information) and dielectric permittivity measurements (Figure S1c, Supporting Information). The ferroelectricity of **1** is then directly verified by the measurements of “double wave method” (Figure S1d, Supporting Information) and calculated by a simple point charge model (Table S2, Supporting Information).

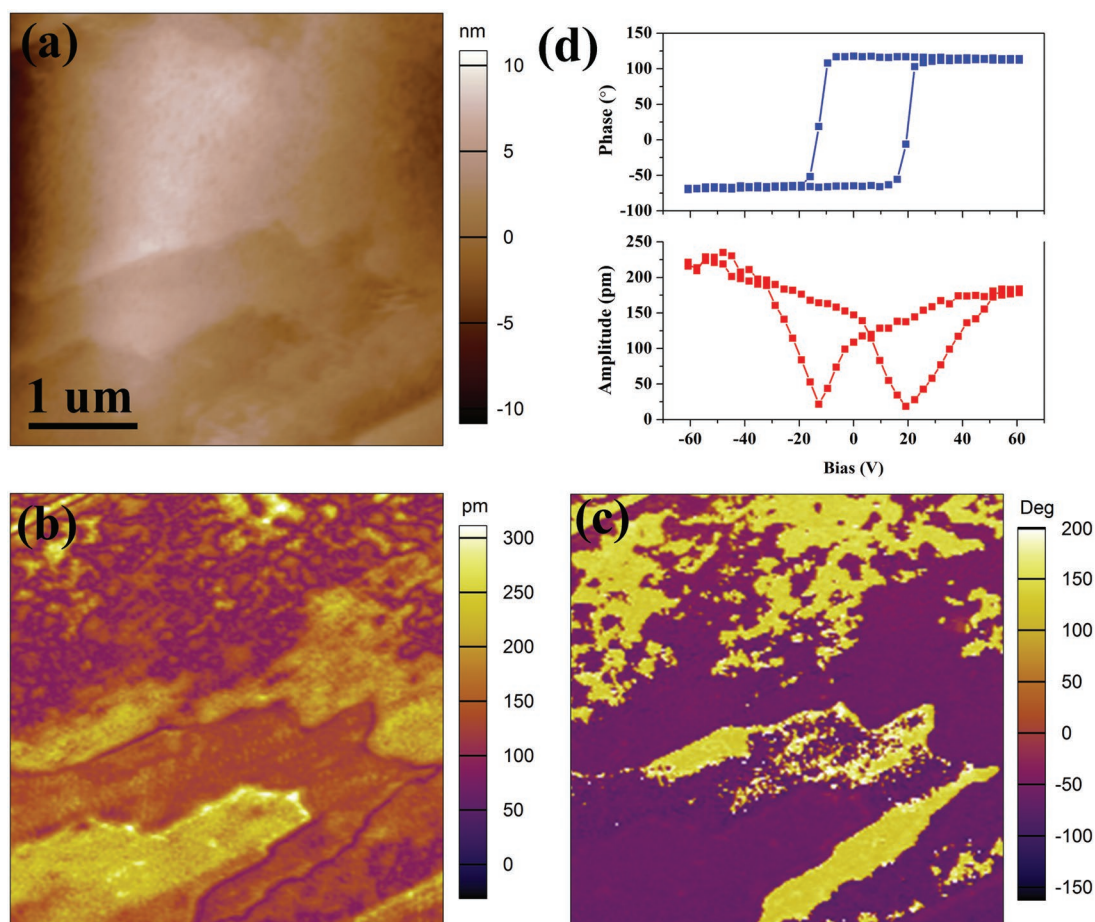


**Figure 2.** Measured domain structure of (DFCHA)<sub>2</sub>PbI<sub>4</sub> single crystal. a–c) Topography image (a), and corresponding lateral PFM amplitude (b) and phase (c) images of a selected region. d) Local lateral PFM switching spectroscopy of (DFCHA)<sub>2</sub>PbI<sub>4</sub> single crystal.

On the other hand, to further demonstrate the ferroelectric polarization in **1** and analyze the domain structure, microscopic characterization of piezoresponse force microscopy (PFM) was carried out.<sup>[15]</sup> Since the as-grown crystal is in monodomain state, we heated the sample to paraelectric phase and then cooled it down to obtain the multi-domain state. Owing to the structural features of 2D inorganic framework, the cleavage plane of {100} is easily exposed. So the obtained topography of a selected region shows an atomic level roughness and layered morphology (Figure 2a). By monitoring the distortion of cantilever, one can extract piezoresponse signal in both lateral and vertical directions, corresponding to in-plane and out-of-plane polarization, respectively.<sup>[16]</sup> The corresponding in-plane PFM amplitude and phase images are show in Figure 2b,c, respectively. The distinct domain patterns with different shapes are presented in the phase image. The arbitrary shapes of the domains in good agreement with the single polar axis accompany ferroelectric phase transition of *mmmFmm2*. From the amplitude image, domain walls with low contrast can also be clearly observed. Since the polarization of {100} planes is confined within in-plane directions, therefore the out-of-plane PFM response is negligible (not shown). As the characteristic of ferroelectrics, polarization switching is an important evidence, thus we carried out local lateral PFM switching spectroscopy

on the surface of **1**. By applying DC voltage via the conductive tip, the polarization direction of sample underneath could be switched and the phase and amplitude signal was recorded (Figure 2d). The distinct 180° switching of the PFM phase signals with a hysteresis behavior as well as the butterfly-shaped amplitude signals indicate the switchable ferroelectric polarization of **1**, and strongly support our determination of the crystal structure.

To further prove the ferroelectricity and intuitively visualize the polarization switching behaviors of **1**, a direct polarization manipulation was carried out on random sample surface on single crystal. As previously shown, in such a monoaxial ferroelectric material, the polarization direction is confined in plane. First, we performed “angular-resolved PFM”<sup>[17]</sup> by rotating the sample with respect to the cantilever to ensure the polarization direction is perpendicular to the cantilever axis. The as-grown single crystal surface shows a good monodomain state with an in-plane polarization direction (Figure 3e,h). In order to switch the polarization in a direction in-plane, we utilized the trailing field, which is a net electric field vector at the rear side of tip with respect to the tip’s moving direction.<sup>[18]</sup> Once a voltage biased tip is in-contact of the crystal surface, the in-plane component of the stray electric field generated by the PFM tip will switch the

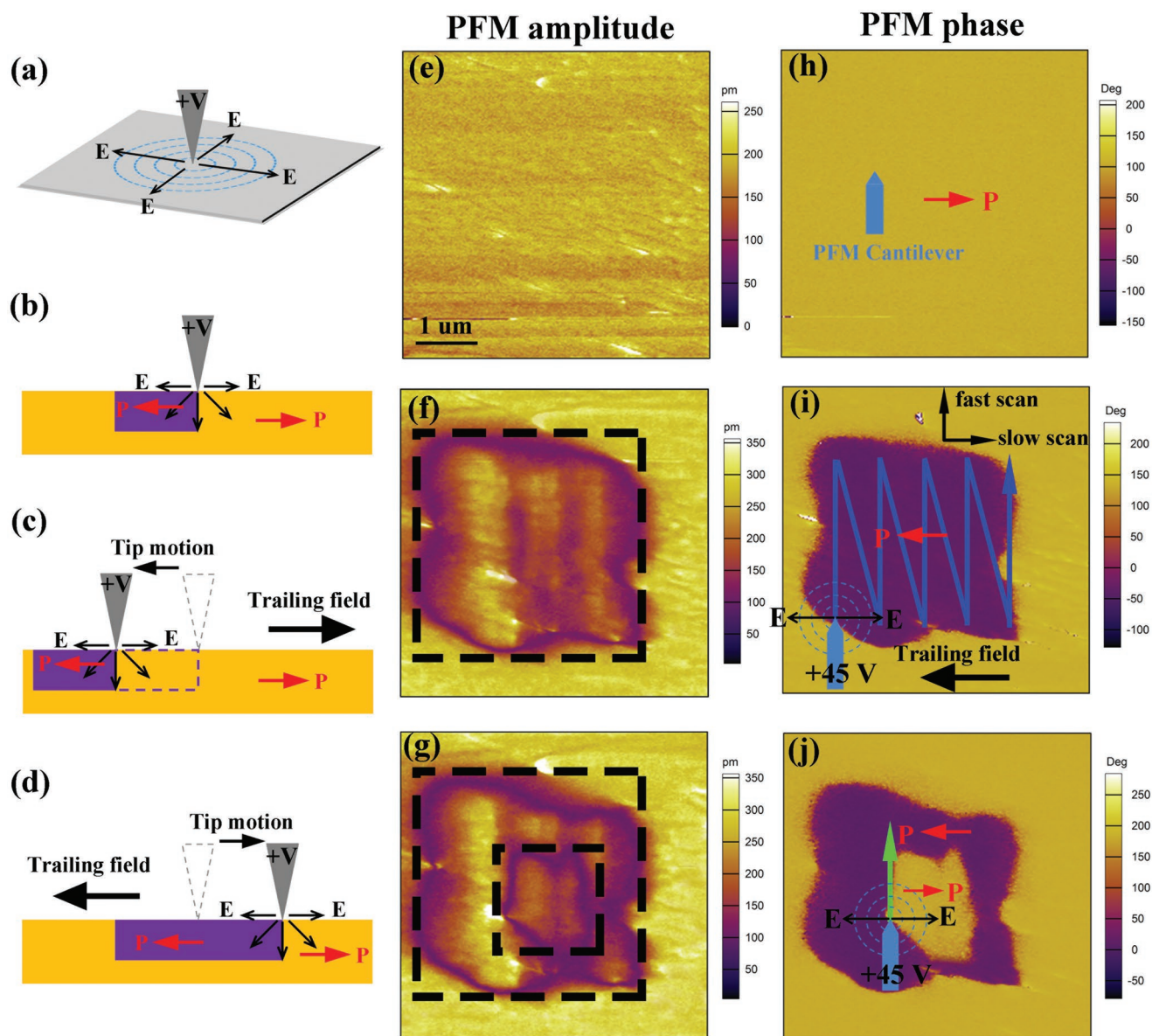


**Figure 3.** Domain switching of  $(\text{DFCHA})_2\text{PbI}_4$  single crystal. a) The distribution of lateral component of the stray electric field created by the positively biased PFM tip. b) Schematic showing the domain switched by the lateral component of tip field. c,d) Schematic showing the domain switched by the front of tip field (c) and the trailing field (d) during the tip motion, respectively. The images in the middle and right columns are PFM amplitude and PFM phase, respectively. e,h) Images for the initial state of the as-grown crystal surface. f,i) Images for the state after the first domain switching operation in the region of the black dashed rectangle, produced by moving the PFM tip along the blue line with the tip bias of +45 V and speed of  $2 \mu\text{m s}^{-1}$ . g,j) Images for the state after the succeeding back-switching operation in the region of the smaller black dashed rectangle, produced by moving the PFM tip along the green arrow with the tip bias of +45 V and speed of  $2 \mu\text{m s}^{-1}$ .

purely lateral domain (Figure 3b).<sup>[19]</sup> With different tip moving direction with respect to the local polarization direction, different polarization switching can be achieved, as illustrated in Figure 3c,d. In our case, when the PFM tip moving along the blue line in Figure 4i with voltage of +45 V and speed of  $2 \mu\text{m s}^{-1}$ , an effective trailing field would switch the polarization to the opposite in-plane polarization.<sup>[20]</sup> Such an in-plane polarization switching was confirmed by PFM imaging. The PFM phase shows an obvious reversal of contrast (Figure 3i) and the domain wall can be observed clearly in the corresponding PFM amplitude image (Figure 3f). To demonstrate

the switching is not permanent but reversible, we moved the PFM tip along the green line in Figure 4j to reverse the polarization again, with voltage of +45 V and speed of  $2 \mu\text{m s}^{-1}$ . Partial domain at right side of the green line, whose polarization direction was opposite to the lateral component of tip field, was switched back (Figure 3g,j). Meanwhile, there are no obvious changes in the topography during the electric poling (Figure S3, Supporting Information). The above PFM data not only proved the existence of the robust ferroelectricity in 1, but also clearly demonstrated the monoaxial nature and switchable in-plane polarization, with a  $180^\circ$  domain wall of

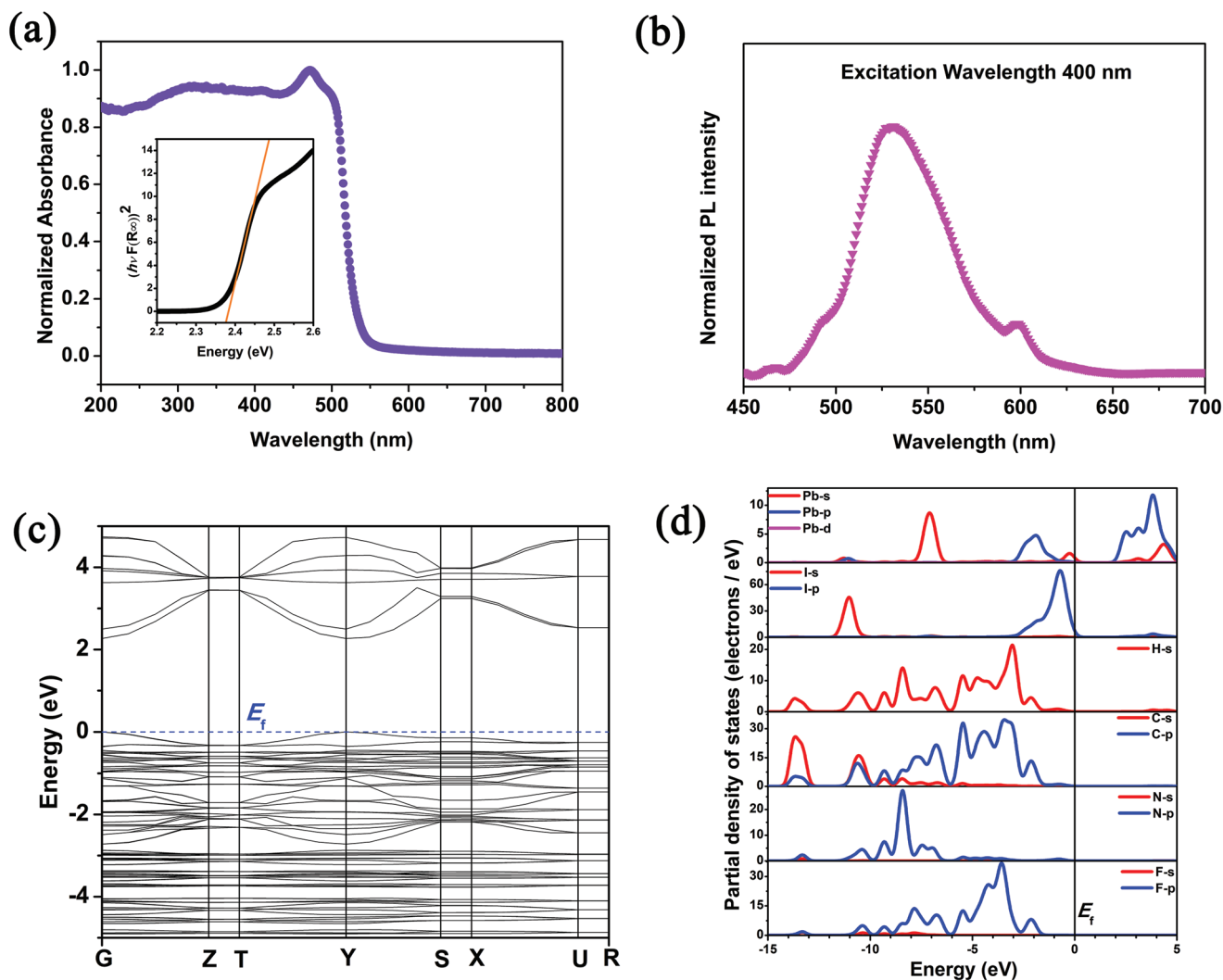


**Figure 4.** a) UV-vis absorption spectrum. b) Fluorescence emission spectrum with 400 nm excitation wavelength. c) Energy band structure. d) The partial density of states (PDOS).

hundreds of nanometers, which attribute 1 a good potential in the in-plane memory device.

As mentioned briefly before, the inorganic framework does not only stabilize the structure, but also determines optical properties. To determine the optical bandgap, UV-vis absorption spectroscopy was carried out on the polycrystalline sample of **1**. As shown in Figure 4a, using variant of the Tauc equation,<sup>[21]</sup> we obtained the bandgap of 2.38 eV. The strong photoluminescence emission (Figure 4b) observed at position of 2.32 eV also indicates the nature of the bandgap is possibly a direct type. To have a deep insight into the electronic structure of **1**, band structure was calculated based on density functional theory (DFT). The conduction band (CB) minimum and the valence band (VB) maximum are localized at the same k-vector in the Brillouin zone (Figure 4c), revealing the direct bandgap nature, which is in good agreement with the sharp UV-vis absorption edge and strong PL emission characteristics. The calculated bandgap is 2.267 eV, which agrees well with the experimental value. Furthermore, the bands can be assigned

according to the partial density of states (PDOS), as plotted in Figure 4d. From PDOS, it is obvious that for the organic part, H-1s states overlap fully with C-2p and N-2p states over almost the whole energy region, indicating the strong covalent interactions in C–H and N–H bonds. For the inorganic part, strong interactions between Pb and I atoms are also found in almost the whole energy region as Pb-s/p and I-s/p states overlap obviously. The bands at the VB top are originated from the non-bonding states of I-5p, and those at the CB bottom are mainly from the unoccupied Pb-5p orbitals. Clearly, both VB maximum and CB minimum are from the electronic states of Pb and I atoms, so it is the inorganic  $\text{PbI}_4$  framework that determines the bandgap of the material.

Finally, we carried out short-circuit photocurrent ( $I_{\text{sc}}$ ) measurement on surface of **1**, to examine the FEPV in such a 2D layered perovskite ferroelectric material. To measure the  $I_{\text{sc}}$ , a picoammeter is directly connected to the two electrodes with no bias voltage applied. Such a configuration allows us to obtain the current generated under light illumination. In

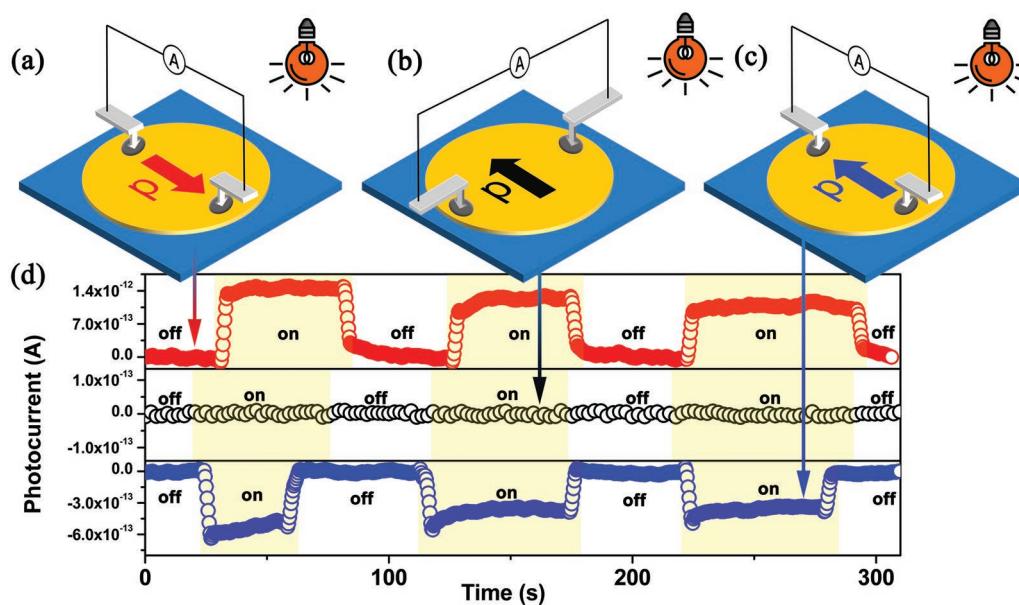


**Figure 5.** a–c) Schematic diagram of FEPV measurement with electrodes aligned parallel (a,c) and perpendicular (b) to the direction of ferroelectric polarization. d) Short-circuit photocurrent in different experimental setup (indicated by different colors), respectively.

order to investigate the polarization-induced photovoltaic effect, a probe station with lamp illumination was employed. The crystallographic orientation of an as-grown crystal was predetermined by PFM measurement, and the measurement was carried out with two In/Ga electrodes aligned parallel/perpendicular to the polarization direction. For the two electrodes aligning parallel to the polarization direction (Figure 5a), finite positive  $I_{sc}$  can be observed under white light (red curve in Figure 5d) with amplitude of  $\approx 1$  pA. In order to eliminate the possibility of the asymmetric electrical potential due to depolarization electric field effects, optical rectification effects, asymmetry of the two electrodes, etc., a large voltage of 130 V was applied on the two electrodes to reverse polarization direction, and  $I_{sc}$  was measured again under the exactly same condition (Figure 5c). This time, due to the reversed polarization, the  $I_{sc}$  obtained became negative in value (as shown in the blue curve in Figure 5d), which clearly demonstrates the relationship of  $I_{sc}$  and the ferroelectric polarization. To further prove the ferroelectric polarization-induced electric field is the origin of  $I_{sc}$  and the existence of FEPV, the same pair of In/Ga electrodes were applied aligning at a direction perpendicular to the ferroelectric polarization (Figure 5b), and no  $I_{sc}$  signal could be detected (as shown in the black curve in Figure 5d). The above results clearly showed that ferroelectric polarization in **1** is the origin of  $I_{sc}$ , and the main mechanism should be FEPV, which promotes the good application potential of **1** as a great candidate in both fundamental study and practical applications.

In summary, we have synthesized the first fluorinated 2D lead iodide perovskite ferroelectrics of **1**. The combination of good ferroelectric properties, 2D perovskite structure and the inorganic framework of lead iodide not only endow **1** with good optical performance, switchable ferroelectric polarization and improved stability, but also make **1** a perfect building block for next generation photovoltaic absorber material and building

block for optoelectronic sensor. More importantly, the confirmed FEPV in this 2D lead iodide perovskite of **1** also makes it a convenient platform to study the effect of ferroelectricity in the newly emerged PSC, which could benefit all related researches and shed light on future optimization of organic solar cells.

## Experimental Section

**Synthesis:** 4,4-Difluorocyclohexylammonium iodide was synthesized by an exactly equimolar mixture of 4,4-difluorocyclohexylamine and HI aqueous solution. Then, 4,4-difluorocyclohexylammonium iodide (20.0 mmol, 5.26 g),  $\text{PbI}_2$  (10 mmol, 4.61 g), and HI aqueous solution (40%, 100 mL) were mixed in a round bottom flask. A clear solution was obtained after refluxing for 3 h at 353 K. Yellow or orange-yellow crystals of **1** were obtained by slowly cooling the solution at a speed of  $0.2 \text{ K h}^{-1}$ . 4,4-difluorocyclohexylamine,  $\text{PbI}_2$ , and HI aqueous solution are commercially available.

**Crystalline Thin Film Preparation:** Single-phase grains of **1** were dissolved in *N,N*-dimethylformamide (DMF) to form a solution with a concentration of about  $300 \text{ mg mL}^{-1}$ . Then,  $20 \mu\text{L}$  of this solution was carefully spread on the prepared commercial ITO-coated glass substrate ( $10 \text{ mm} \times 10 \text{ mm}$ ) and sealed in a clean petri dish by parafilm. With controlled substrate temperature and edge-pinned-crystallization, microcrystalline thin film was fabricated on substrate as the slow evaporation completed.

**Physical Properties Measurement:** Methods of DSC, SHG, dielectric, fluorescence emission spectrum, and UV–vis spectrum were described elsewhere.<sup>[22]</sup>  $P$ – $E$  hysteresis loops measurements were recorded using the double-wave method at 298 K. The double-wave method was carried out on a tabletop cryogenic probe station (Lake Shore, Model PS-100) and parameter analyzer (Keithley 4200A-SCS).

**X-Ray Crystallographic Measurements:** Single-crystal structure was measured with Rigaku Saturn 924 CCD diffractometer and  $\text{Mo-K}\alpha$  radiation ( $\lambda = 0.71073 \text{ \AA}$ ) at 298 and 398 K, respectively. CCDC Number 1904976 and 1904977 containing the crystallographic data can be downloaded free of charge from The Cambridge Crystallographic Data Centre via [www.ccdc.cam.ac.uk/data\\_request/cif](http://www.ccdc.cam.ac.uk/data_request/cif).

**PFM Measurements:** PFM measurements were carried out on a commercial atomic force microscope (Asylum Research MFP-3D) under the resonance-enhanced mode. Conductive Pt/Ir-coated silicon probes were used for PFM lithography.

## Supporting Information

Supporting Information is available from the Wiley Online Library or from the author.

## Acknowledgements

T.-T.S., Y.-A.X., and Q.P. contributed equally to this work. This work was supported by the National Natural Science Foundation of China (21427801), the Natural Science Foundation of Jiangsu Province (BK20160029) and the Fundamental Research Funds for the Central Universities

## Conflict of Interest

The authors declare no conflict of interest.

## Keywords

ferroelectric photovoltaic effect, lead halide perovskites, molecular ferroelectrics, perovskite ferroelectrics

Received: March 23, 2019

Revised: April 30, 2019

Published online: June 6, 2019

- [1] a) Z. Xiao, Y. Yuan, Y. Shao, Q. Wang, Q. Dong, C. Bi, P. Sharma, A. Gruverman, J. Huang, *Nat. Mater.* **2015**, *14*, 193; b) M. V. Kovalenko, L. Protesescu, M. I. Bodnarchuk, *Science* **2017**, *358*, 745; c) Y.-M. You, W.-Q. Liao, D. Zhao, H.-Y. Ye, Y. Zhang, Q. Zhou, X. Niu, J. Wang, P.-F. Li, D.-W. Fu, Z. Wang, S. Gao, K. Yang, J.-M. Liu, J. Li, Y. Yan, R.-G. Xiong, *Science* **2017**, *357*, 306; d) B. Saparov, D. B. Mitzi, *Chem. Rev.* **2016**, *116*, 4558.
- [2] A. Kojima, K. Teshima, Y. Shirai, T. Miyasaka, *J. Am. Chem. Soc.* **2009**, *131*, 6050.
- [3] NREL, <https://www.nrel.gov/pv/cell-efficiency.html> (accessed: May 2019).
- [4] a) W. Q. Liao, D. W. Zhao, Y. Yu, N. Shrestha, K. Ghimire, C. R. Grice, C. L. Wang, Y. Q. Xiao, A. J. Cimaroli, R. J. Ellingson, N. J. Podraza, K. Zhu, R. G. Xiong, Y. F. Yan, *J. Am. Chem. Soc.* **2016**, *138*, 12360; b) D. W. Zhao, Y. Yu, C. L. Wang, W. Q. Liao, N. Shrestha, C. R. Grice, A. J. Cimaroli, L. Guan, R. J. Ellingson, K. Zhu, X. Z. Zhao, R. G. Xiong, Y. F. Yan, *Nat. Energy* **2017**, *2*, 7; c) F. Hao, C. C. Stoumpos, D. H. Cao, R. P. H. Chang, M. G. Kanatzidis, *Nat. Photonics* **2014**, *8*, 489.
- [5] H. H. Tsai, W. Y. Nie, J. C. Blancon, C. C. S. Toumpos, R. Asadpour, B. Harutyunyan, A. J. Neukirch, R. Verduzco, J. J. Crochet, S. Tretiak, L. Pedesseau, J. Even, M. A. Alam, G. Gupta, J. Lou, P. M. Ajayan, M. J. Bedzyk, M. G. Kanatzidis, A. D. Mohite, *Nature* **2016**, *536*, 312.
- [6] J. M. Frost, K. T. Butler, F. Brivio, C. H. Hendon, M. van Schilfgarde, A. Walsh, *Nano Lett.* **2014**, *14*, 2584.
- [7] a) J. Seidel, D. Y. Fu, S. Y. Yang, E. Alarcon-Llado, J. Q. Wu, R. Ramesh, J. W. Ager, *Phys. Rev. Lett.* **2011**, *107*, 4; b) S. Y. Yang, J. Seidel, S. J. Byrnes, P. Shafer, C. H. Yang, M. D. Rossell, P. Yu, Y. H. Chu, J. F. Scott, J. W. Ager III, L. W. Martin, R. Ramesh, *Nat. Nanotechnol.* **2010**, *5*, 143; c) T. Choi, S. Lee, Y. J. Choi, V. Kiryukhin, S. W. Cheong, *Science* **2009**, *324*, 63.
- [8] a) B. Chen, T. Li, Q. Dong, E. Mosconi, J. Song, Z. Chen, Y. Deng, Y. Liu, S. Ducharme, A. Gruverman, F. De Angelis, J. Huang, *Nat. Mater.* **2018**, *17*, 1020; b) E. Strelcov, Q. Dong, T. Li, J. Chae, Y. Shao, Y. Deng, A. Gruverman, J. Huang, A. Centrone, *Sci. Adv.* **2017**, *3*, e1602165.
- [9] a) T. A. Berhe, W.-N. Su, C.-H. Chen, C.-J. Pan, J.-H. Cheng, H.-M. Chen, M.-C. Tsai, L.-Y. Chen, A. A. Dubale, B.-J. Hwang, *Energy Environ. Sci.* **2016**, *9*, 323; b) J.-P. Correa-Baena, M. Saliba, T. Buonassisi, M. Graetzel, A. Abate, W. Tress, A. Hagfeldt, *Science* **2017**, *358*, 739.
- [10] Z. Wang, Q. Lin, F. P. Chmiel, N. Sakai, L. M. Herz, H. J. Snaith, *Nat. Energy* **2017**, *2*, 17135.
- [11] F. Zhang, D. H. Kim, H. Lu, J.-S. Park, B. Larson, J. Hu, L. Gao, C. Xiao, O. Reid, X. Chen, Q. Zhao, P. F. Ndione, J. J. Berry, W. You, A. Walsh, M. C. Beard, K. Zhu, *J. Am. Chem. Soc.* **2019**, *141*, 14.
- [12] a) H.-Y. Ye, W.-Q. Liao, C.-L. Hu, Y. Zhang, Y.-M. You, J.-G. Mao, P.-F. Li, R.-G. Xiong, *Adv. Mater.* **2016**, *28*, 2579; b) W.-Q. Liao, Y. Zhang, C.-L. Hu, J.-G. Mao, H.-Y. Ye, P.-F. Li, S. D. Huang, R.-G. Xiong, *Nat. Commun.* **2015**, *6*, 7338.
- [13] Z. Zhang, P.-F. Li, Y.-Y. Tang, A. J. Wilson, K. Willets, M. Wuttig, R.-G. Xiong, S. Ren, *Sci. Adv.* **2017**, *3*, 8.
- [14] K. Aizu, *J. Phys. Soc. Jpn.* **1969**, *27*, 387.
- [15] a) A. Gruverman, M. Alexe, D. Meier, *Nat. Commun.* **2019**, *10*, 1661; b) R. K. Vasudevan, N. Balke, P. Maksymovych, S. Jesse, S. V. Kalinin, *Appl. Phys. Rev.* **2017**, *4*, 021302; c) J. Li, J.-F. Li, Q. Yu, Q. N. Chen, S. Xie, *J. Materiomics* **2015**, *1*, 3.
- [16] E. N. Esfahani, T. Li, B. Huang, X. Xu, J. Li, *Nano Energy* **2018**, *52*, 117.
- [17] L. You, F. Liu, H. Li, Y. Hu, S. Zhou, L. Chang, Y. Zhou, Q. Fu, G. Yuan, S. Dong, *Adv. Mater.* **2018**, *30*, 1803249.
- [18] A. Crassous, T. Sluka, A. K. Tagantsev, N. Setter, *Nat. Nanotechnol.* **2015**, *10*, 614.
- [19] a) A. V. Ievlev, D. O. Alikin, A. N. Morozovska, O. V. Varenik, E. A. Eliseev, A. L. Kholkin, V. Y. Shur, S. V. Kalinin, *ACS Nano* **2015**, *9*, 769; b) H. Lu, T. Li, S. Poddar, O. Goit, A. Lipatov, A. Sinitskii, S. Ducharme, A. Gruverman, *Adv. Mater.* **2015**, *27*, 7832.
- [20] N. Balke, S. Choudhury, S. Jesse, M. Huijben, Y. H. Chu, A. P. Baddorf, L.-Q. Chen, R. Ramesh, S. V. Kalinin, *Nat. Nanotechnol.* **2009**, *4*, 868.
- [21] J. Tauc, R. Grigorov, A. Vancu, *Phys. Status Solidi B* **1966**, *15*, 627.
- [22] a) P.-F. Li, W.-Q. Liao, Y.-Y. Tang, H.-Y. Ye, Y. Zhang, R.-G. Xiong, *J. Am. Chem. Soc.* **2017**, *139*, 8752; b) Y.-Y. Tang, P.-F. Li, W.-Y. Zhang, H.-Y. Ye, Y.-M. You, R.-G. Xiong, *J. Am. Chem. Soc.* **2017**, *139*, 13903; c) H.-Y. Ye, J.-Z. Ge, Y.-Y. Tang, P.-F. Li, Y. Zhang, Y.-M. You, R.-G. Xiong, *J. Am. Chem. Soc.* **2016**, *138*, 13175; d) Y. Zhang, W.-Q. Liao, D.-W. Fu, H.-Y. Ye, Z.-N. Chen, R.-G. Xiong, *J. Am. Chem. Soc.* **2015**, *137*, 4928.